Supersonic-Jet Experiments Using a High-Energy Laser

B. Loupias, M. Koenig, Emeric Falize, Serge Bouquet, Norimasa Ozaki, Alessandra Benuzzi-Mounaix, Tommaso Vinci, Claire Michaut, M. Rabec Le Gloahec, W. Nazarov, et al.

Supersonic-Jet Experiments Using a High-Energy Laser

B. Loupias,[1,*] M. Koenig,[1] E. Falize,[2,3] S. Bouquet,[2,3] N. Ozaki,[1,4] A. Benuzzi-Mounaix,[1] T. Vinci,[1] C. Michaut,[3] M. Rabec le Goahec,[1] W. Nazarov,[5] C. Courtois,[2] Y. Aglitskiy,[6] A. Ya. Faenov,[7] and T. Pikuz[7]

[1]*LULI, Ecole Polytechnique, CNRS, CEA, UPMC, Route de Saclay, 91128 Palaiseau, France*
[2]*CEA/DIF/DPTA BP 12, 91680 Bruyeres-le-Chatel, France*
[3]*Laboratoire de l'Univers et de ses Théories, Observatoire de Paris, CNRS, Université Paris Diderot, Place Jules Janssen, 92190 Meudon, France*
[4]*Graduate School of Engineering, Osaka University, Suita, Osaka 565-0871, Japan*
[5]*School of Chemistry, University of St Andrews, Purdie Blg, St Andrews KY16 9ST, United Kingdom*
[6]*Science Applications International Corporation, McLean, Virginia 22102, USA*
[7]*Joint Institute for High Temperatures of RAS, Izhorskaya 13/19, Moscow, 125412, Russia*

(Received 6 August 2007; published 26 December 2007)

In this Letter, laboratory astrophysical jet experiments performed with the LULI2000 laser facility are presented. High speed plasma jets (150 km · s^{-1}) are generated using foam-filled cone targets. Accurate experimental characterization of the plasma jet is performed by measuring its time evolution and exploring various target parameters. Key jet parameters such as propagation and radial velocities, temperature, and density are obtained. For the first time, the required dimensionless quantities are experimentally determined on a single-shot basis. Although the jets evolve in vacuum, most of the scaling parameters are relevant to astrophysical conditions.

DOI: 10.1103/PhysRevLett.99.265001 PACS numbers: 52.72.+v, 52.50.Lp, 52.70.La, 98.38.Fs

High-energy density facilities, such as high power lasers or Z pinches, enable the exploration of extreme states of matter as found in several astrophysical objects. Using appropriate diagnostics, measurements of such conditions and their time evolution allow to validate and to test theoretical models and simulation codes [1]. This approach has been already used to perform plasma jets studies [2–4]. Astrophysical jet dynamics are affected by many physical phenomena such as radiation [5,6], magnetic fields [7], and interaction with interstellar medium [8]. The complexity of jet evolution theories and simulations needs comparisons with controlled data. For that reason laboratory experiments help to answer basic questions like, for instance, how do some jets stay collimated over the large distances observed?

In this Letter, we show it is possible to launch a supersonic jet with a new flexible target (see Fig. 1) which can be used with any high-energy long pulse laser facility. To control and to accurately diagnose the jet, it is generated at the rear side of the target. For jets created on the laser side as in [9], their interaction with the laser beam can induce spurious effects and modify their evolution [10]. This also removes options for exploring jet propagation in ambient media. This point is of special interest to produce plasma jets which can be scaled to astrophysical ones, i.e., in such a way to be hydrodynamically and radiatively similar to their astrophysical counterpart. Similarity constraints are achieved if dimensionless numbers for laboratory jets have the same order of magnitude as astrophysical ones [11]. The Mach number (M), the cooling parameter (χ), and the jet-to-ambient density ratio (η) describe global properties of jets. For a fluid description of plasmas, Reynolds (R_e) and Peclet (P_e) numbers as well as the localization parameter (δ) have to be evaluated. The key point for an astrophysical experiment is the determination of all these parameters, and we measured the jet velocity V_{jet}, its radial evolution [$R(t)$ and V_R], temperature $T_{\text{jet}}(t)$, and electronic density $n_e(t)$ to achieve this goal. Time-resolved diagnostics have been used to investigate evolution of these quantities, which is a required income to validate models.

The two LULI2000 kJ nanosecond beams were converted to the second harmonic to drive a strong shock through the foam as described in Fig. 1. The beams were focused with a 500 μm focal spot diameter and the pulse duration was 1.5 ns (square), giving a maximum intensity $I_L \approx 10^{14}$ W/cm^2. The shock was generated in a two layer target. A first 20 μm plastic (CH) layer acts as ablator-

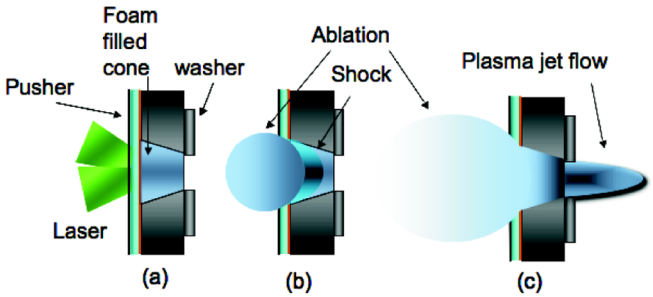

FIG. 1 (color online). Foam-filled cone target process. The cone entrance has a 500 μm diameter (exit diameter 100 μm) and thickness is 250 μm. (a) The laser is focused on the pusher. (b) It drives a shock into the foam. (c) The shock is guided in the cone and a high velocity plasma jet flow is generated.

pusher and a 3 μm thick Ti layer prevents x-ray preheating of the foam. Then the shock propagates through the foam and generates a dense and hot plasma [12]. The conical shape guides, confines, and accelerates the plasma flow onto the symmetry axis, producing a supersonic jet. To vary initial conditions and to study their effects on the jet collimation, we used two different foam densities, 50 mg/cm^3 and 100 mg/cm^3. A 100 μm long washer at the cone exit was added on some shots in order to enhance collimation. When performing x-ray radiographies (see below), foam was doped with high Z material to increase contrast.

The experimental setup is shown in Fig. 2. In the transverse direction (perpendicular to the propagation axis), we implemented visible shadowgraphy and VISAR (Velocity Interferometer System for Any Reflector) diagnostics using a 20 ns low power probe beam (532 nm). As a rear side diagnostic, the VISAR is commonly used in equation of state experiments to measure shock velocity [13]. In our scheme, the probe laser goes through the hot plasma and is then split and temporally delayed in the two arms of the VISAR. When recombined we obtain an interferogram providing the plasma refractive index time variation. By recording the fringe shift evolution, we obtain the electron density gradient $dn_e(t)/dt$ below the critical value n_c. On the target rear side, we set up a Self Optical Pyrometry (SOP) [14]. To determine T_{jet}, we adopted here an absolute photon counting technique to get the equivalent blackbody temperature. Finally, to probe the jet core density, a transverse 2D x-ray radiograph at 5 keV (Heα vanadium line) was implemented using a spherical bent crystal [15,16] to get monochromatic high spatially resolved images of the jets. A 8 μm spatial resolution was achieved along the plasma flow axis, which was measured on test shots using 400-lines-per-inch gold grids.

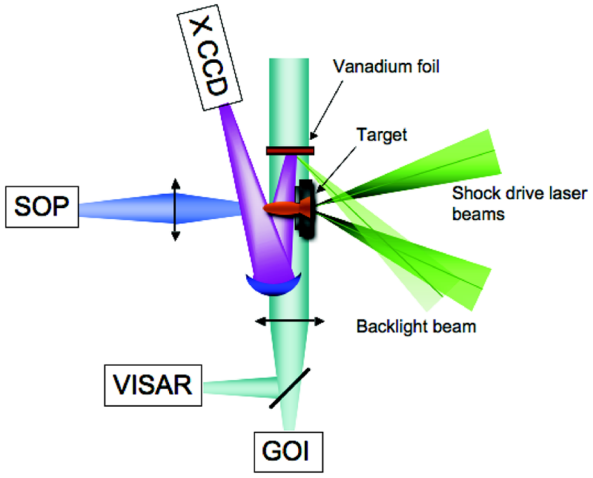

FIG. 2 (color online). Schematic view of the experimental setup. For the x-ray diagnostic, one of the two beams is used as backlighter.

Among the jet parameters listed above, velocity is crucial as it appears in each dimensionless number. Therefore an accurate measurement is required and has been achieved with the transverse VISAR. When $n_e \approx n_c/10$, the probe beam is absorbed and refracted so no light is collected by the camera as shown in Fig. 3. The slope of the frontier between transmitted and absorbed light (dashed line) provides V_{jet} that ranges from 100 to 150 km $\cdot$ s^{-1} depending on laser intensity, foam density, and presence of washer. About 8 ns after the main laser a fringe shift, due to a low density plasma (transparent to visible light), occurs ahead of the absorbing zone. This plasma develops at the jet front at high velocity ($\approx$175 km/s). By a temporal integration of the fringe shift, we deduced the electron density of this plasma to be $n_e \approx 8 \times 10^{18}$ cm^{-3}. Around 11 ns after the main laser, this plasma has a 100 μm extension ahead of the absorbing zone of the jet, representing only 10% of its total length.

The second set of parameters [radial evolution $R(t)$, V_R and temperature $T_{\text{jet}}(t)$] can be derived from the SOP diagnostic. Indeed, when the shock breaks out from the foam, early emission from the plasma located in the washer (Fig. 4) is detected. The diameter of the plasma is kept to 100 μm during 1 ns, the traveling time of the flow through the washer. When the jet emerges into vacuum, it radially expands. By successive radial lineouts, jet radius time evolution $R(t)$ and its velocity $V_R(t)$ are deduced, and for the shot presented in Fig. 4, $V_R(t) \approx 35$ km/s. From the SOP we were also able to determine the jet temperature time evolution. Along the central region of the self-emission ($R = 0$ μm) we first observe a maximum temperature due to the shock breakout at the end of the cone. Then at the washer exit, the jet temperature is 3 eV and

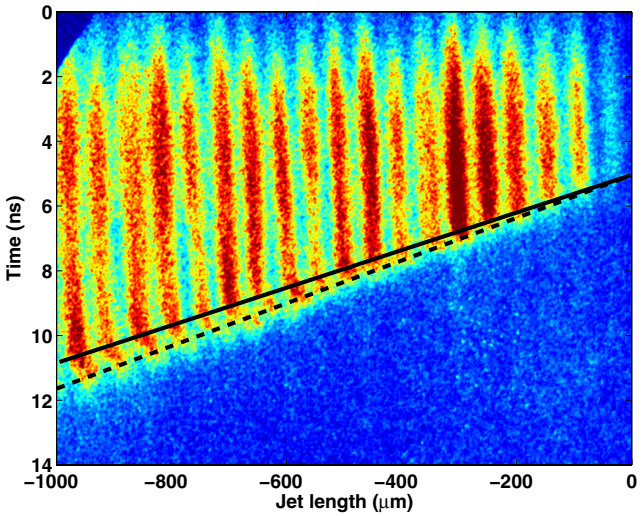

FIG. 3 (color online). VISAR interferogram for a target with washer and 50 mg/cm^3 foam. The dashed line slope provides jet velocity. The solid line defines the beginning of fringe shift showing to a low density expanding plasma ahead of the jet bulk.

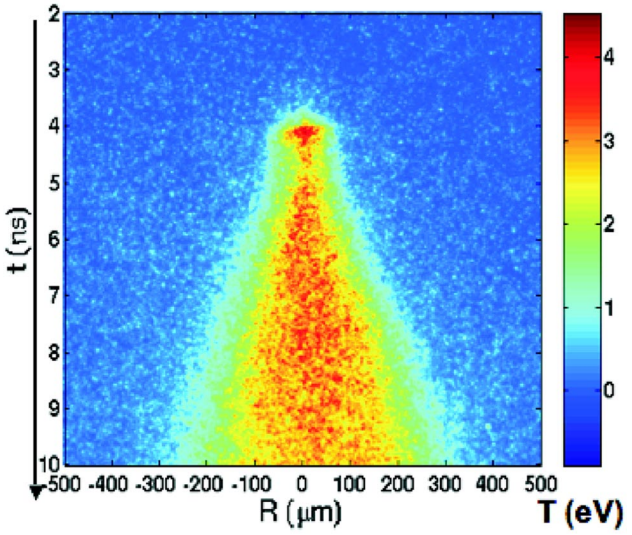

FIG. 4 (color online). Temperature of the jet given by the SOP diagnostics.

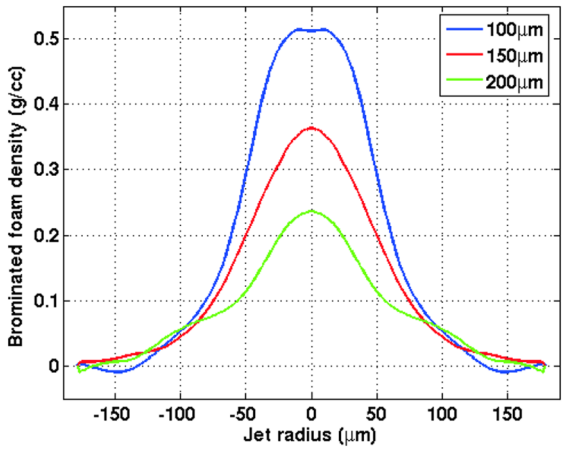

FIG. 5 (color online). Radial density profile of the jet at 100 μm, 150 μm, and 200 μm. It is extracted from the x-ray radiography for 50 mg/cm^3 foam density 12 ns after the main laser time.

remains quite constant for 5 ns. One notices that the observed self-emission comes from a region close to a fraction of the critical density. Indeed, the small low density plasma ahead of the jet, mentioned above, does not absorb the light recorded on the SOP (at 450 nm). Moreover as described below, the hot foam plasma is expected to be fairly uniform both for the temperature and the density, implying that the measured temperature is the actual jet temperature within our error bars $\approx \pm 10\%$. If we consider now the radial profile of the temperature at different times, we notice a top hat profile, the edges of which slightly decrease with time. The jet cools radially due to its expansion in vacuum and radiation losses.

For a complete scaling of the jet, we need to determine its density, but visible diagnostics provide only a fraction of n_c. The jet core density measurement is achieved by using x-ray radiography diagnostic and Beer's law, $I = I_0 \exp(-\mu_m \overline{\rho d})$ that gives the transmitted x-ray intensity, I, after propagation through the jet at density ρ and with a diameter d. Figure 5 shows radial density profiles of the jet along the propagation axis. Because of radial symmetry, an Abel inversion was performed to extract the density assuming a brominated foam absorption given by the cold case. At these low temperatures (a few eV), bromine opacities are not expected to be different from cold ones for high-energy x rays (5 keV). At 100 μm from the cone exit, a density $\rho = 0.5$ g/cm^3 was measured which corresponds to a compression factor $\rho/\rho_0 \approx 10$. To go further into the plasma characterization, we performed, in addition to x-ray radiography, visible shadowgraphy of the plasma flow to determine the jet shape at much lower density. A beam splitter was placed in front of the VISAR to obtain a 2D image using two Gate Optical Imagers having a 120 ps integration time. For the 2D pictures taken early in time, we observed a plasma jet with radial extension $R \approx 100$ μm corresponding to the washer exit tip radius, but later (see Fig. 6) the jet diameter becomes larger, reaching ≈ 500 μm at half of its total length (≈ 850 μm). The radial evolution of the plasma can be described analytically using Euler equations with a polytropic pressure law. As expected, due to the high value of $V_{\text{jet}}(t) \approx$ 100–150 km/s, the jet remains quite collimated late after the main drive beams, which was confirmed by comparing the two Gate Optical Imager results for the same shot at two different times. Considering the set of these data, we were able to compute most of the fundamental jet parameters (see Table I) with different initial conditions. We observe that when a washer was added, V_{jet} increased while the radial expansion was slightly reduced. This clearly shows that the washer did guide efficiently the plasma flow and also enhanced the jet collimation. These effects are observed using both transverse shadowgraphy and

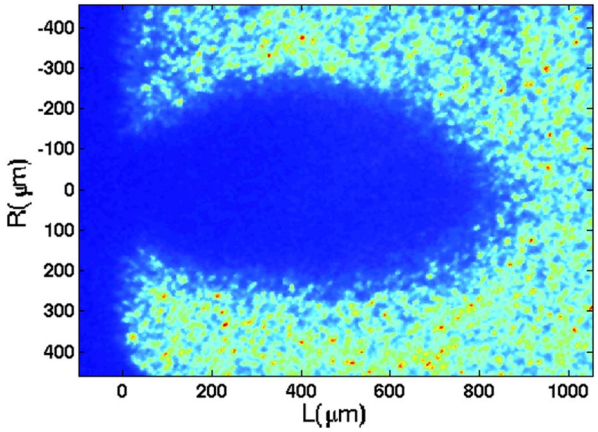

FIG. 6 (color online). Transverse shadowgraphy of the jet 11 ns after the main laser beam.

TABLE I. Jet parameters.

Foam density (mg/cm^3)	T_{jet}(eV)	V_{jet}(km · s^{-1})	V_R(km · s^{-1})	M	P_e	R_e	χ
50	3.2	122	52	9.2	1×10^5	4×10^8	5×10^3
100	2	99	33	9.4	4×10^5	1.4×10^9	3×10^4
50[a]	3	144	35	11	1.3×10^5	5.4×10^8	6×10^3
100[a]	1.9	110	32	10.7	5×10^5	2×10^9	4×10^4
astrophysical jet	a few eV	100—300	a few $km.s^{-1}$	≈ 10	$\gg 1$	$\gg 1$	0.1–10

[a]With washer.

self-emission diagnostics for our initial densities (50 and 100 mg/cm^3); a faster but also cooler jet with higher aspect ratio was obtained by adding a washer.

As shown previously and reported in Table I, T_{jet}, V_{jet}, ρ, and n_e measurements allowed calculations of dimensionless numbers. For Peclet and Reynolds numbers, respectively $P_e = \text{Rc}_s/\kappa$ and $R_e = \text{RV}_{\text{jet}}/\nu$ with c_s the sound velocity, we used the Spitzer formulae [17] for viscosity (ν) and thermal diffusivity (κ). The localization parameter, δ (also relevant for astrophysical jet but not presented in the table), was calculated, $\delta < 10^{-6}$, confirming the collisional aspect of the plasma. Moreover, from the cooling parameter, $\chi = \tau_{\text{rad}}/\tau_{hydro}$, which compares the radiative time (τ_{rad}) to the hydrodynamic one ($\tau_{\text{hydro}} = R/c_s$), we can estimate the importance of the radiative flux in the jet dynamic. Using blackbody law as lower limit for τ_{rad}, radiation does not have a big role in jet cooling, as χ is large compared to one. Nevertheless, we can compare our plasma jets to Herbig Haro objects [18], which are thought to be nonrelativistic collimated bipolar outflows resulting from the existence of accretion disks during the star formation process. Some very detailed observations of evolutionary changes have been made, such as the knots motion along the plasma jet. Typical astrophysical jet parameters are $M \approx 10$, $P_e \gg 1$, $R_e \gg 1$, and $\chi \approx 0.1$–10 (see Table I), and, therefore, the possibility to generate high Mach number low temperature jets having good similarities with astrophysical jets using a new target scheme is demonstrated in this paper. However, as they evolve into vacuum and are optically thick, χ is larger than for Herbig Haro ones. To reduce this value, we expect to be able to generate hotter plasma by changing, for example, the foam characteristics: very low density, high Z material, and by optimizing laser conditions to the cone shape. It would hence be possible to increase radiative losses and decrease the value of χ. Future experiments will consider all these aspects and, especially, interaction with an ambient medium to approach realistic astrophysical situations leading to appropriate value of η. Astronomical observations and theories highlight the role of the magnetic field during the jet generation and propagation. The dimensionless parameter to consider is therefore β, which corresponds to the ratio of thermal pressure to magnetic pressure ($\beta = P_{\text{th}}/P_B$). Close to the star ($\lesssim 10^3$ AU), the ambient electronic density and the ambient magnetic field are rather high ($n \gtrsim 10^3$ cm^{-3} and $B \gtrsim 100$ μG, respectively) so $\beta \approx$ a few units. At large distance, d, from the star ($d \gtrsim 10^4$ AU), B^2 decreases faster than n; consequently $\beta \approx \frac{n}{B^2}$ increases up to a few 10s as reported in [19]. Considering our jet measurements and using devices currently in development, we could expect generated magnetic fields up to 1 MG providing $\beta \gtrsim 0.4$. The achievable range of variation in the magnetic field (0 G up to 1 MG) is very promising to investigate experimentally its effects on various jet regimes, i.e., jet propagation close to far from the star.

*berenice.loupias@polytechnique.fr

[1] B. A. Remington, P. R. Drake, and D. D. Ryutov, Rev. Mod. Phys. **78**, 755 (2006).
[2] S. V. Lebedev *et al.*, Plasma Phys. Controlled Fusion **47**, B465 (2005).
[3] J. M. Foster *et al.*, Astrophys. J. **634**, L77 (2005).
[4] D. R. Farley *et al.*, Phys. Rev. Lett. **83**, 1982 (1999).
[5] J. M. Blondin *et al.*, Astrophys. J. **360**, 370 (1990).
[6] J. Grun *et al.*, Laser Part. Beams **21**, 529 (2003).
[7] K. Tsinganos *et al.*, Astrophys. Space Sci. **287**, 103 (2003).
[8] T. A. Movsessian *et al.*, Astron. Astrophys. **470**, 605 (2007).
[9] K. Shigemori *et al.*, Phys. Rev. E **62**, 8838 (2000).
[10] A. D. Edens *et al.*, Phys. Plasmas **11**, 4968 (2004).
[11] D. Ryutov *et al.*, Astrophys. J. **518**, 821 (1999).
[12] M. Koenig *et al.*, Phys. Plasmas **6**, 3296 (1999).
[13] P. M. Celliers *et al.*, Rev. Sci. Instrum. **75**, 4916 (2004).
[14] M. Koenig *et al.*, Phys. Plasmas **10**, 3026 (2003).
[15] Y. Aglitskiy *et al.*, Appl. Opt. **37**, 5253 (1998).
[16] T. Pikuz *et al.*, Laser Part. Beams **22**, 289 (2004).
[17] L. Spitzer *et al.*, *Physics of Fully Ionized Gases*, Interscience Tracts on Physics and Astronomy (Interscience, New York, 1962), 2nd ed..
[18] B. Reipurth *et al.*, Annu. Rev. Astron. Astrophys. **39**, 403 (2001).
[19] P. Hartigan *et al.*, Astrophys. J. **661**, 910 (2007).